Strain effects on the thermal conductivity of nanostructures

Xiaobo Li, Kurt Maute, Martin L. Dunn, and Ronggui Yang[*]

Department of Mechanical Engineering, University of Colorado, Boulder, Colorado 80309-0427, USA

(Received 20 December 2009; revised manuscript received 26 May 2010; published 18 June 2010)

Applying stress/strain on a material provides a mechanism to tune the thermal conductivity of materials dynamically or on demand. Experimental and simulation results have shown that thermal conductivity of bulk materials can change significantly under external pressure (compressive stress). However, stress/strain effects on the thermal conductivity of nanostructures have not been systematically studied. In this paper, equilibrium molecular-dynamics (EMD) simulation is performed to systematically study the strain effects on the lattice thermal conductivity of low-dimensional silicon and carbon materials: silicon nanowires (one dimensional) and thin-films (two dimensional), single-walled carbon nanotube (SWCNT, one dimensional) and single-layer graphene sheet (two dimensional). Spectral analysis of EMD is further developed and then applied to avoid the numerical artifacts such as the neglect of long-wavelength phonons that are often encountered when using EMD with periodic boundary conditions. Intrinsic thermal conductivity of the simulated bulk and nanostructures can be obtained using spectral analysis of EMD. The thermal conductivity of the strained silicon and diamond nanowires and thin films is shown to decrease continuously when the strain changes from compressive to tensile. However, for SWCNT and single-layer graphene, the thermal conductivity has a peak value, and the corresponding applied strain is at −0.06 or −0.03 for SWCNTs depending on the chirality and at zero for graphene, respectively. The following two reasons could explain well the effects of strains on the thermal conductivity of the nanowires and thin films that decreases continuously from compressive strain to tensile strain: (1) mode-specific group velocities of phonons decrease continuously from compressive strain to tensile strain and (2) the specific heat of each propagating phonon modes decrease continuously from compressive strain to tensile strain. However, for SWCNT and single-layer graphene, the mechanical instability induces buckling phenomenon when they are under compressive strains. The phonon-phonon scattering rate increases significantly when the structure buckles. This results in the decreasing behavior of thermal conductivity of SWCNT and graphene under compressive stress and explains the peak thermal conductivity value observed in SWCNT and single-layer graphene when they are under strain. The results obtained in this paper has important implications of challenging thermal management of electronics using advanced materials such as carbon nanotubes and graphene. It also points to a potentially new direction of dynamic thermal management.

I. INTRODUCTION

The advances in nanotechnology have resulted in novel materials and devices with much smaller length scales but enhanced functionality. Thermal transport in these low-dimensional nanostructures (two-dimensional: thin films and superlattices, one-dimensional: nanowires (NWs) and nanotubes, zero-dimensional: quantum dots, and the bulk form of low-dimensional materials: nanocomposites) (Refs. [1–6]) has been an interesting research topic over the past two decades due to the intriguing electron and phonon physics in the low-dimensional materials, the ever-increasing challenges in the thermal management,[7–9] and the potentials in using nanostructures for enhanced energy conversion, storage, and thermal management.[10–12] Significant developments on both experimental characterization and theoretical studies have been achieved along with reasonably good understanding of how the thermal conductivity of nanostructures changes as a function of constituent materials, crystal structures, grain boundary and interfaces, defects and impurity, dimensionality, and size.

Such an understanding has recently led to another rather interesting but less-explored research area—tuning the thermal conductivity for superior performance, either statically or dynamically, inspired by the working principle of the workhorse of integrated circuits—metal-oxide-semiconductor field-effect transistor (MOSFET), which are essentially a variable electrical resistor that is tunable under an electrical field. Intensive research efforts have been directed toward thermal rectifiers in which heat can flow in one direction while it is prohibited in the opposite direction and significant applications have been imagined.[13–17] Among many possibilities that could either statically or dynamically tune thermal transport, stress/strain effects, and geometric in symmetry could be the most obvious way to exercise. Indeed stress and strain effects on material properties (electrical, optical, and mechanical) have been explored with a long history. Strained silicon is used to enhance the electron mobility in MOSFETs.[18–20] Strain/stress effects on optical properties can be also used for reducing the threshold carrier density and thus increasing the gain of laser diodes.[21–23] Recently, there are also great interests in using strains to tune the quality factor of nanowire resonators.[24] Strain/stress effects can also be used to enhance the performance of thermoelectric materials,[25,26] which is indeed a combination of strain/stress effects on electrical and thermal transport properties. All the aforementioned suggest the potential of using stress/strain to tune the thermal conductivity. Such a tuning mechanism which could be either applied dynamically or statically could result in significant impacts on addressing thermal management challenges in electronics and exploring the nanoen-

abled energy solutions. On the other hand, the effects of stress/strain on the thermal conductivity of nanostructures need to be understood well for repeatable thermal characterization and the design of nanostructures since materials and devices are almost always under compressive or tensile strains in both practical applications and experimental characterization.

Indeed considerable number of measurements have been made for the thermal conductivity of various liquids and solids in bulk form under pressure up to a few gigapascals around 1970s and 1980s or even earlier.[27–33] Ross, *et al.*[27] concluded that the thermal conductivity of semiconductors increases with pressure (compressive strain). They explained the pressure effects on thermal conductivity increases from the phonon velocity increase under pressure for semiconductors. Interestingly the authors also reported a very small decrease (1% at 0.7 GPa) for silicon under uniaxial stress and they concluded this change as not substantial. Equilibrium molecular dynamics (EMD) has been conducted to show that the thermal conductivity of solid argon increases with a decreasing molar volume (or an increasing pressure).[34] Picu, *et al.*[35] studied the nonhydrostatic strain-induced thermal-conductivity anisotropy and attributed the difference to lattice anharmonicity. Bhowmicka, *et al.*[36] derived the relationship of thermal conductivity as a function of temperature and strain using the Peierls-Boltzmann formulation. The results show a power-law scaling of thermal conductivity on temperature and strain. Scattered studies of the strain effects on the thermal conductivity of nanostructures have also been reported.[37–39] Fan, *et al.* calculated the thermal conductivity of single-walled carbon nanotube (SWCNT) under 150 MPa compression and under 500 MPa tension using nonequilibrium MD (NEMD). They showed an increasing thermal conductivity with increasing compression pressure and a decreasing thermal conductivity with increasing tensile stress, which is in the same trend as Lennard-Jones solids.[37] Abramson, *et al.*[38] studied a strained bilayer thin film and showed that the effective thermal conductivity can be less than half of the average thermal conductivity of the corresponding unstrained thin films only. Rosenblum, *et al.*[39] studied thermal stress effects on thermal conductivity of diamond thin film on substrate with MD simulation. A decreased thermal conductivity is obtained under compressive strain. They conclude that two factors affect the thermal conductivity: (1) compressive stress shifts the maximum frequency upwards in the phonon spectrum and thus increases the frequency region in which phonons can propagate. The thermal conductivity will thus increase under compressive strain. (2) However, stress-induced defects serve as additional mechanism of phonon scattering, which decreases the thermal conductivity. Overall thermal conductivity decreases under compressive strain since the effect of defect-induced reduction is much stronger. A rather thorough study of literature inspired us to systematically study the strain effects on the thermal conductivity of bulk and nanostructured semiconductors including carbon nanotubes and single-layer graphene sheet since the existing data are not conclusive: (1) very few study, both experimentally and theoretically, exists on the dependence of thermal conductivity of tensile strains. (2) The scattered studies of strain effects on thermal conductivity of nanostruc-

tures have been over simplified, for example, using simple interatomic potentials such as the Lennard-Jones potential that could model very limited material systems. (3) Often these studied are complicated with numerical artifacts that are associated with the methods used. (4) Comparing to thin films and nanowires, possible new phenomena such as buckling could be expected for carbon nanotubes and graphene, due to the extreme thin-layer nature of the materials. But whether the bucking affects the thermal conductivity has not been reported.

In this work, we use EMD to study the strain effects on the lattice thermal conductivity of silicon and carbon bulk and nanostructures including silicon NWs (one dimensional) and thin films (two dimensional), SWCNT (one dimensional) and single-layer graphene sheet (two dimensional). EMD simulations of thermal conductivity usually show strong non-physical simulation size dependence due to the cutoff of long-wavelength (low-frequency) phonons. To eliminate these nonphysical artifacts, in Sec. II we further developed the spectral analysis method[40] and demonstrate the applicability of this method for the thermal-conductivity analysis of low-dimensional structures. In Sec. III, we present systematic studies of the strain effects on silicon and carbon nanostructures (silicon and diamond nanowire and thin film, SWCNT, single graphene sheet) using the EMD along with the spectral analysis method. The contributions of this work could be summarized as: (1) further development of spectral analysis of EMD which avoids numerical artifacts in small simulation domains when using periodic boundary conditions. (2) Systematic study of the dependence of thermal conductivity on both compressive and tensile strains for bulk and nanostructured semiconductors. This is the first quantitative study in literature with very detailed explanations for the findings. (3) An exception of the thermal conductivity dependence on compressive strains is observed in single-layer structures (carbon nanotubes and graphene) from semiconductor thin films and nanowires. We found that the competition mechanisms in enhancing and reducing thermal conductivity when applying compressive strains results in a peak thermal conductivity of these single-layer carbon nanostructures at certain compressive strains.

II. SIMULATION METHODS

Several statistical and atomistic approaches can potentially be used to study strain effects on thermal conductivity of nanostructures, such as Boltzmann transport equation (BTE), nonequilibrium Green's function (NEGF),[41] and MD simulation. BTE has the potential to study large system but needs strain-dependent phonon-dispersion curves and phonon mean-free path, which could be a daunting job. When considering anharmonic interaction, NEGF can be another way to study strain effects on thermal conductivity. However this approach becomes difficult to implement when the anharmonic interaction is involved. MD is an efficient way to study strain effects on thermal conductivity due to the easiness in implementing strains on the atomistic system. Both NEMD and EMD can possibly be used to study strain effects on thermal conductivity. Here EMD method is applied due to

its simplicity in the way of applying strain, which will be discussed in Sec. III. In general, MD has its intrinsic drawbacks in addressing long-wavelength phonons. In this section, we present our further development of the spectral analysis which addresses the intrinsic numerical artifacts.

A. Equilibrium molecular dynamics

In MD, the trajectory of particles (molecular, atoms, etc.) in a simulation domain is tracked by solving Newton's equation of motion.[42] Particles interact with each other through empirical interatomic potentials which are usually developed from quantum force-field calculations. In our simulation, the initial atomic positions are generated based on the crystal structures. The initial velocity is generated by using the Box-Muller method[43] followed by a step which sets the translational and angular momentum of the collective motion to zero. Force exerted on each particle is calculated from the derivative of empirical interatomic potential. Velocity Verlet algorithm[44] is used to integrate Newton's equation of motion with a set time step of 1 fs. The temperature of simulation domain is then brought to 300 K by rescaling the velocity of each particle and the simulation domain is then relaxed by performing 250 ps simulation in NVE (constant number of particles, volume, and energy) ensemble to reach a fully equilibrium state. From the linear-response theory, thermal conductivity can be calculated using Green Kubo's relation under equilibrium state. In an anisotropic material, it is given by the tensor form[45,46]

$$k_{ij} = \frac{1}{k_B V T^2} \int_0^\infty \langle S_i(t) \cdot S_j(0) \rangle dt, \tag{1}$$

where k_B is Boltzmann constant, V is volume, T is temperature, S is heat current, and $\langle S_i(t) \cdot S_j(0) \rangle$ is called heat current autocorrelation function (HCACF). For an isotropic material, the thermal conductivity is represented by the main axis value,

$$k = \frac{1}{3k_B V T^2} \int_0^\infty \langle \mathbf{S}(t) \cdot \mathbf{S}(0) \rangle dt. \tag{2}$$

For materials with high thermal conductivity such as silicon and diamond, the HCACF converges slowly and a long simulation time is required. In our simulation, simulation time from 20 to 60 ns is used for the direct integral from Eq. (1) or (2). Also the calculated thermal conductivity with Eq. (1) or (2) usually shows strong initial condition (the initial velocity) dependence, so each simulation is repeated five times with different initial condition and the final result is obtained by averaging the obtained values.

Both Stillinger-Webber (SW) (Ref. 47) and Tersoff[48] empirical potential have been widely used in MD simulations of silicon and carbon systems. Usually Stillinger-Weber potential can provide better agreement of thermal properties with experiments than Tersoff potential, such as melting temperature and thermal-expansion coefficient.[49–52] However SW potential was built based on the ideal tetrahedral bond angle and its applicability is limited. For example, SW potential fails in the prediction of the correct energies for silicon under high pressure and it does not correctly predict surface structures in which nontetrahedrally bonds are present.[53,54] We therefore chose Tersoff potential in our study.

Usually the lattice constant predicted from empirical potential is not the same as experimental data for bulk material.[50,52] In order to determine the lattice constant of a strain-free bulk material, simulations are performed by calculating the pressure of the system when varying preset lattice constant under periodic boundary conditions in three directions. By linear fitting of the pressure-lattice constant plot, lattice constant of a strain-free structure can be determined at the zero pressure value. This procedure is validated by applying it on bulk silicon and the results agree well with Ref. 52. By applying Tersoff potential, the lattice constant determined for a free-standing structure is 5.446 Å for bulk Si and 3.572 Å for bulk diamond, comparing with the experimental value 5.431 Å and 3.567 Å, respectively.[55]

B. Spectral analysis of EMD

In the Green Kubo's relation, an upper limit integration time is usually set to evaluate the integral. If the HCACF decays to zero value at a relatively short time,[34,56,57] direct integral method can be applied to calculate the thermal conductivity. However for some materials (i.e., silicon, diamond, silicon carbide, etc.),[58–61] the HCACF decays to zero with a very long tail which could be up to 100 ps and a much longer total simulation time is needed to obtain a well-converged HCACF (could be up to 20 ns). In comparison with 1 fs time step, such a long simulation time makes the simulation rather expensive to evaluate thermal conductivity from the direct integral method. Che *et al.*[59] suggested using exponential decay function to fit the HCACF function,

$$\langle \mathbf{S}(t) \cdot \mathbf{S}(0) \rangle = A_o e^{-t/\tau_o} + A_a e^{-t/\tau_a}, \tag{3}$$

where, o and a indicate optical phonons and acoustic phonons. Thermal conductivity can then be evaluated using the fitting parameters A_o, A_a, τ_o, and τ_a,

$$k = \frac{1}{3k_B V T^2} (A_o \tau_o + A_a \tau_a). \tag{4}$$

Although the periodic boundary condition is applied in EMD, thermal-conductivity results obtained from the above methods still show strong simulation size dependence.[62] The reason is that phonons with a wavelength greater than twice of the simulation-domain size will be cut off. With an increasing simulation-domain size, more long-wavelength modes are included and thus the calculated thermal conductivity increases and becomes closer to its true value.

Based on the above analysis, spectral methods have been proposed to eliminate the cutoff artifacts due to the finite simulation size,[40,63] and the method described by Chen *et al.*[40] is adopted here. From Ref. 40, Fourier transform of HCACF is taken and the frequency-dependent thermal conductivity can be written as

$$k(\omega) = \frac{1}{3k_BVT^2} \int_0^\infty \langle \mathbf{S}(t) \cdot \mathbf{S}(0) \rangle e^{i\omega t} dt. \quad (5)$$

By taking the zero-frequency limits, Eq. (5) restores to the much simpler Green-Kubo formula [Eq. (2)]. This shows that the conventional thermal conductivity can be expressed as: $k = k(\omega)|_{\omega=0}$, which is also called the static thermal conductivity.

For low-frequency phonons with a frequency lower than the simulation-domain cutoff frequency, the corresponding frequency-dependent thermal-conductivity data is not accurate. Data at higher frequency are then used to extrapolate the zero-frequency limit thermal conductivity. To perform the spectral fitting, Eq. (3) can be used to model the HCACF. In previous studies with spectral methods, only continuous HCACF is used in the formulation of Eq. (5), which is only valid if τ_o and τ_a are far greater than the simulation time step and far smaller than the HCACF upper limit integration time. Considering that in MD simulation, only a discrete set of HCACF data is generated with a certain simulation time step, the HCACF can be expressed as

$$\langle \mathbf{S}(t) \cdot \mathbf{S}(0) \rangle_{\text{Des}} = A_s e^{-n\Delta t/\tau_s} + A_l e^{-n\Delta t/\tau_l}, \quad 0 \le n \le N-1, \quad (6)$$

where N is the total HCACF data collecting steps, Δt is time step ($t = n\Delta t$), and s, l are used to describe short and long relaxation time, respectively, instead of o and a in a general way. The Fourier transform of Eq. (6) is then,

$$F\{\langle \mathbf{S}(t) \cdot \mathbf{S}(0) \rangle_{\text{Des}}\}$$
$$= \Delta t \sum_{n=0}^{N-1} [A_s e^{-n\Delta t/\tau_s} + A_l e^{-n\Delta t/\tau_l}] \exp(-in\omega\Delta t). \quad (7)$$

The summation in Eq. (7) can be calculated and the frequency-dependent thermal conductivity can then be written as

$$k(\omega) = \frac{\Delta t}{3k_BVT^2} \left| \sum_{i=s,l} \frac{A_i[1 - \exp(-N\Delta t/\tau_i)]}{1 - \exp(-\Delta t/\tau_i)\exp(-i\omega\Delta t)} \right|. \quad (8)$$

If $N\Delta t \gg \tau \gg \Delta t$, Eq. (8) can be simplified as

$$k(\omega) = \frac{1}{3k_BVT^2} \left| \frac{A_s \tau_s}{1 + i\omega\tau_s} + \frac{A_l \tau_l}{1 + i\omega\tau_l} \right|. \quad (9)$$

The frequency-dependent thermal conductivity basically denotes how each phonon modes are excited and their contributions to the overall heat transport. Volz[64] studied the frequency-dependent thermal conductivity of Si and found that the effective thermal conductivity from 10 GHz to 1 THz is about 1.1 W/(m K) at 200 K and 1.7 W/(m K) at 500 K, much lower than the conventional (static) thermal conductivity if the material is thermally excited at such high frequency. Our analysis gives a similar value of around 1.3 W/(m K) at 300 K in the same frequency range for Si. Recently, Cahill *et al.*,[65] experimentally showed that the thermal conductivity of semiconductor alloy thin films can change significantly with the modulation heating frequency.
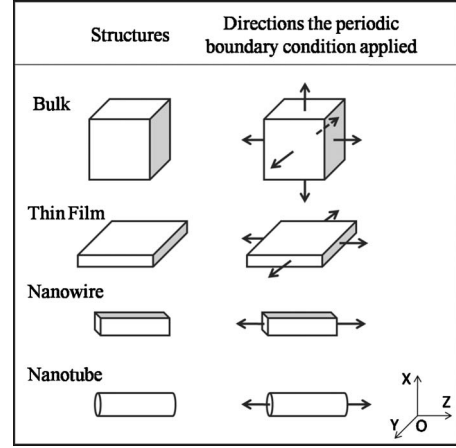

FIG. 1. Illustration of the directions in which the periodic boundary conditions are applied for a variety of structures studied in this paper. Strain is applied in the same direction that has an infinite size, i.e., where the periodic boundary condition is applied.

In this paper, our interest is on how to obtain the conventional (static) thermal conductivity through the data fitting process using the frequency-dependent relaxation (thermal conductivity). In the above discussions, the parameters (A_s, τ_s) that are related to phonons with short relaxation time converges at a relatively short simulation time and they could be fitted directly from HCACF. Parameters (A_l, τ_l) that are related to phonons with long relaxation time is then fitted with Eq. (8). With the obtained fitting parameters A_s, τ_s, A_l, τ_l, the static thermal conductivity can be obtained,

$$k = k(\omega)|_{\omega=0} = \frac{1}{3k_BVT^2}(A_s \tau_s + A_l \tau_l). \quad (10)$$

The spectral method for obtaining simulation-domain size-independent thermal conductivity have been performed and validated for bulk materials in past studies. In this work, this method is further applied to low-dimensional systems and the validations are presented below.

C. Validation

To validate the EMD with spectral analysis, we studied the thermal conductivity of bulk silicon and diamond along [100] direction. We note that thermal conductivity along other directions could be simulated but we expect similar trends in other directions. Two different simulation domains are used for calculating the thermal conductivity of bulk silicon: cubic simulation domains with $N \times N \times N$ unit-cells cuboid simulation domains with $4 \times 4 \times N$ unit cells at X, Y, and Z directions, respectively, while the calculation for bulk diamond is shown for cubic simulation domains with $N \times N \times N$ unit cells only. As shown in the first row of Fig. 1, periodic boundary conditions are used by repeating the original simulation domains in all directions for bulk materials. To calculate the thermal conductivity, we averaged thermal conductivity values at X, Y, and Z directions the $N \times N \times N$ simulation domain while only the value at Z direction is used for $4 \times 4 \times N$ simulation domain.
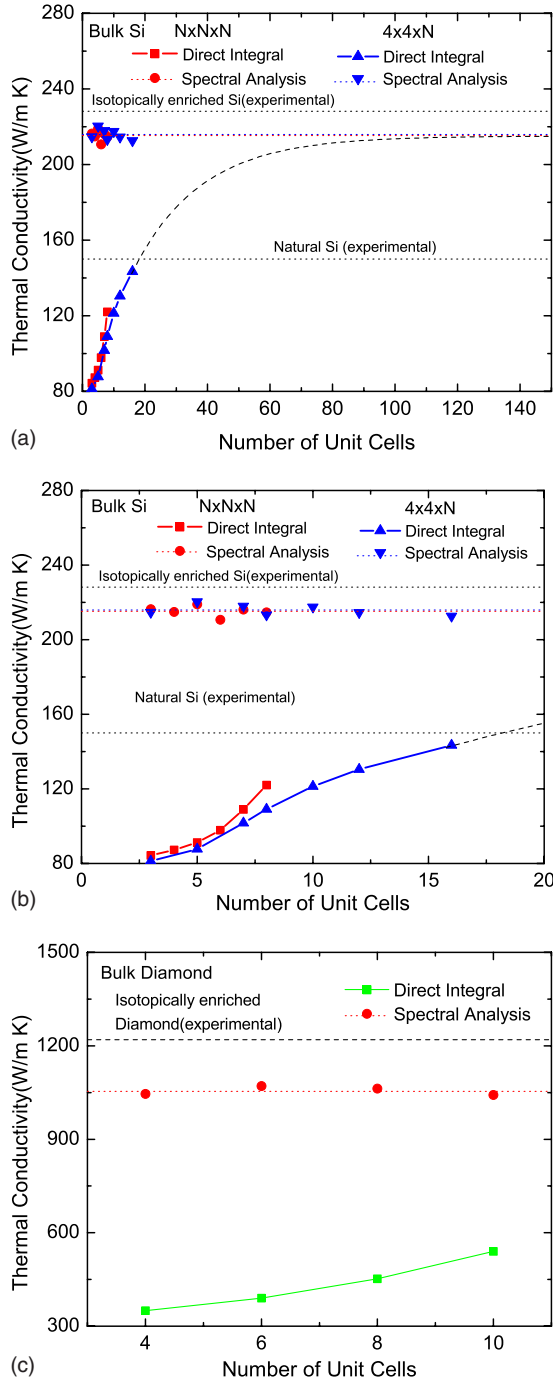
(a)

(b)

(c)

FIG. 2. (Color online) Thermal conductivity of: [(a) and (b)] bulk silicon and (c) bulk diamond, calculated by direct integral method and spectral analysis method using EMD. Simulation domains are cubic one with $N \times N \times N$ unit cells and cuboid one with $4 \times 4 \times N$ unit cells at X, Y, and Z directions, respectively. Periodic boundary conditions are applied in three directions. Dashed lines are exponential fitting using Eq. (11). Experimental data are taken from Refs. 66 and 67.

Figure 2 shows that thermal conductivity obtained from the direct integral method has strong simulation-domain dependence. By using spectral analysis, simulation-domain-independent thermal conductivity can be extrapolated for simulation domains with both $N \times N \times N$ and $4 \times 4 \times N$ unit
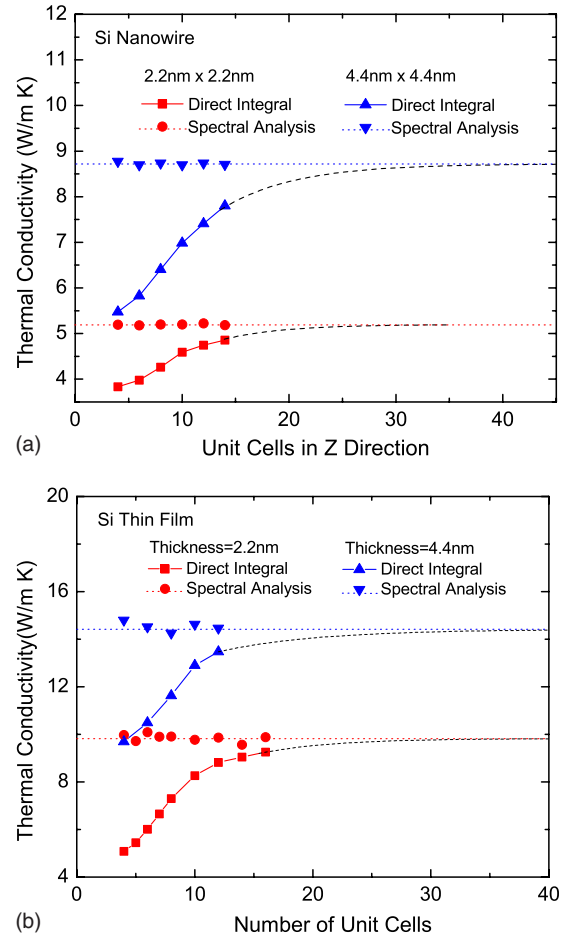
FIG. 3. (Color online) (a) Thermal conductivity of silicon nano-wires in the axial direction. (b) In-plane thermal conductivity of silicon thin films. Results from direct integral and spectral method are both shown. Dashed lines are exponential fitting using Eq. (11).

cells, which further proves that a smaller simulation domain can be used for thermal-conductivity calculation with spectral method. For comparison, we also showed the experimental thermal-conductivity value of natural Si and isotopically enriched Si (Ref. 66) and isotopically enriched diamond[67] in the figure. The results from spectral analysis give good agreements with experiment results.

In the Green Kubo's relation in Eq. (2), an upper limit integration time t_0 is usually set to evaluate the integral, instead of time ∞. t_0 is proportional to the size of the simulation domain with a rough estimation of $t_0 \sim N/v_p$, where N is number of unit cells and v_p is mean phonon velocity.[68] By integrating Eq. (2) from 0 to t_0 with the approximated format of the HCACF function shown in Eq. (3), the thermal conductivity can then be expressed as

$$k = k_\infty - B \exp(-N/C), \qquad (11)$$

where B and C are related to the long relaxation time, and k_∞ is the converged thermal conductivity if the simulation-domain size is infinite since the exponential function in Eq. (3) with short relaxation time converges fast and it gives a constant value when substituted into the integral Eq. (2).
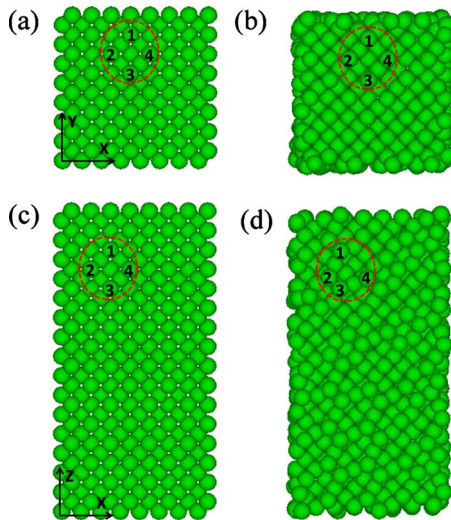
FIG. 4. (Color online) Surface reconstruction of Si nanowire. Periodic boundary condition is applied in the Z direction (along the wire axis): [(a) and (b)] XY cross-sectional surface structure before and after the simulation; [(c) and (d)] XZ surface structure before and after the simulation. Same atoms are labeled with the same number (1, 2, 3, and 4) in (a) and (b), or (c) and (d).

Equation (11) indicates that the thermal conductivity from the EMD with direct integral method will converge at its intrinsic bulk value if one could increase the size of the simulation domain to an extent that the long-wavelength cut-off is not significant for thermal conductivity. However it will be too computationally costly for convergence study of simulation domains with $N \times N \times N$ unit cells, we have thus conducted a convergence study for periodic simulation domains with Si with $4 \times 4 \times N$ unit cells. Fitting results gives good agreement with the thermal conductivity obtained from EMD with spectral analysis. This further confirms that the EMD with spectral analysis is able to obtain results without numerical artifacts. The thermal conductivity value from direct integral converges to 99.9% of the one from the spectral method with a length of 76.5 nm for $4 \times 4 \times N$ unit cells. The length of the simulation domain, 76.5 nm, is much longer than the wavelength of dominant thermal transport phonons, 1 nm, and in the same order of the mean-free path of those phonons, 10–300 nm for silicon at room temperature. How the converged simulation-domain size is correlated with the thermal transport dominant phonon wavelength and phonon mean-free path will be a worthful topic to explore in the future, but beyond the scope of this work.

To study the thermal conductivity of low-dimensional nanostructures, periodic boundary condition is only applied in the unconstrained directions as shown in Fig. 1. For thin film, one direction (noted as X direction) is constrained and periodic boundary conditions are applied in Y and Z directions. To calculate the thermal conductivity in the in-plane direction, the HCACF is summated in Y and Z main axes and the average value is used. For nanowires, periodic boundary condition is applied only in Z direction and the HCACF is summated in Z axis. We also note that the Z axis of all the silicon and carbon structures with diamond lattice shown in Fig. 1 are aligned along the [100] direction.
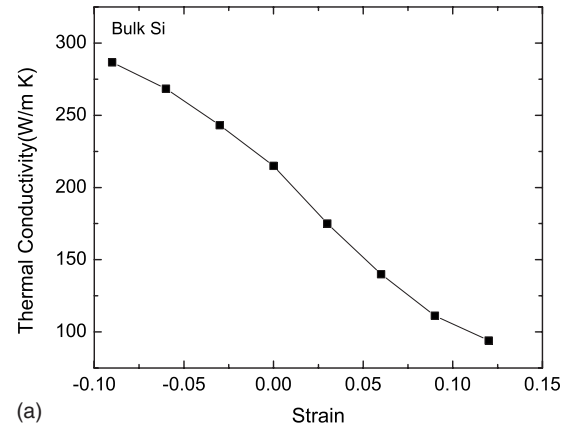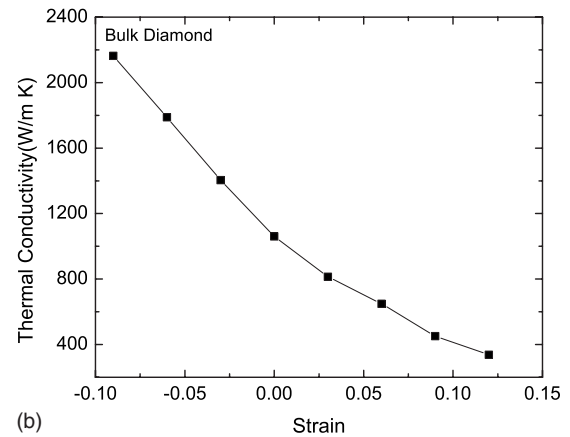
FIG. 5. Strain effects on the thermal conductivity of: (a) bulk silicon and (b) bulk diamond.

The same spectral method has been applied to study the thermal conductivity of Si thin films and Si nanowires and the results are given in Fig. 3. It shows that for both low-dimensional materials, spectral method can avoid the artifacts of simulation-domain dependence of the direct integral method. For silicon nanowire, NEMD simulation with Stillinger-Weber potential predicted a thermal conductivity of 2.35 W/m K for a 2.2 nm×2.2 nm Si nanowire and 6.86 W/m K for a 4.3 nm×4.3 nm one,[69] which is comparable with our EMD prediction considering the different potentials we used. By exponential fitting with Eq. (11), thermal conductivity of the direct integral method converges at a value obtained from the spectral method when the simulation-domain size is larger than ∼25 nm. The requirement of small simulation-domain size for integral method to converge might have something to do with the apparent mean-free path of phonons, which will be shorter in nanostructures than in its bulk form.

In the simulation of nanowires and thin films, the atoms have dangling bonds at the surfaces where free boundary condition is used and these atoms are in an unstable state. These atoms will recombine with each other to form new bonds, which are usually referred as surface reconstructions. In our simulation, surface reconstruction is also observed, which is shown in Fig. 4. It clearly shows that at the surface (XY surface) where periodic condition is applied, the atomic positions are the same before and after the simulation. How-
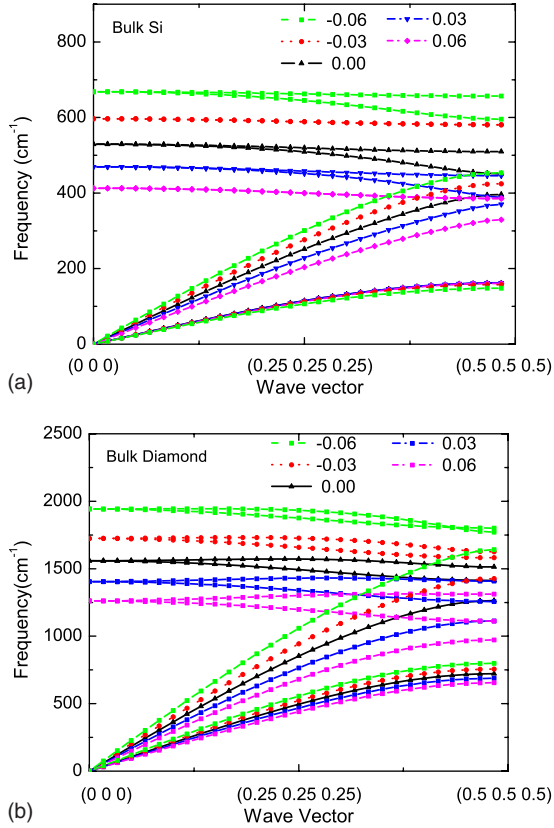
FIG. 6. (Color online) Phonon-dispersion curves of: (a) bulk silicon and (b) bulk diamond under different strain ("−" denotes compressive strain and "+" denotes tensile strain).

FIG. 7. (Color online) Normalized specific heat of: (a) bulk silicon and (b) bulk diamond under different strain (− denotes compressive strain and + denotes tensile strain). All the data are normalized to the saturated specific heat with zero strain at high temperature.

ever, at the constrained surface (*XZ* surface), reconstruction happens. In Fig. 4(d), it clearly shows that the spacing between atoms 2 and 3 becomes smaller and a new bond forms between them. Surface reconstruction results in a different structure than that of the bulk materials and it can scatter phonons significantly, which greatly reduces the thermal conductivity of low-dimensional materials (i.e., nanowires and thin films).

It is worth noting that the divergent thermal conductivity has been reported for low-dimensional systems in literature.[70] The divergent thermal conductivity studied in Ref. 70 and recent works by others, mostly result from ideal one-dimensional chains or two-dimensional lattices with relatively simple potential forms, such as Lennard-Jones potential and Fermi-Pasta-Ulam potential. This study focuses on more practical nanostructures such as nanowires and thin films, which are indeed three dimensional in the computational domain, with empirical potentials that give converging thermal conductivity results. Past work using EMD on similar material systems studied in this paper show that the simulation-domain size-dependent artifact exists but converging results are possible with large computational cost by increasing the simulation-domain size. This work eliminates the simulation-domain size artifact to obtain converged results from a small simulation domain with spectral analysis.

III. RESULTS AND DISCUSSIONS

In this section, we will discuss the effects of the applied strain on the thermal conductivity of silicon and carbon in
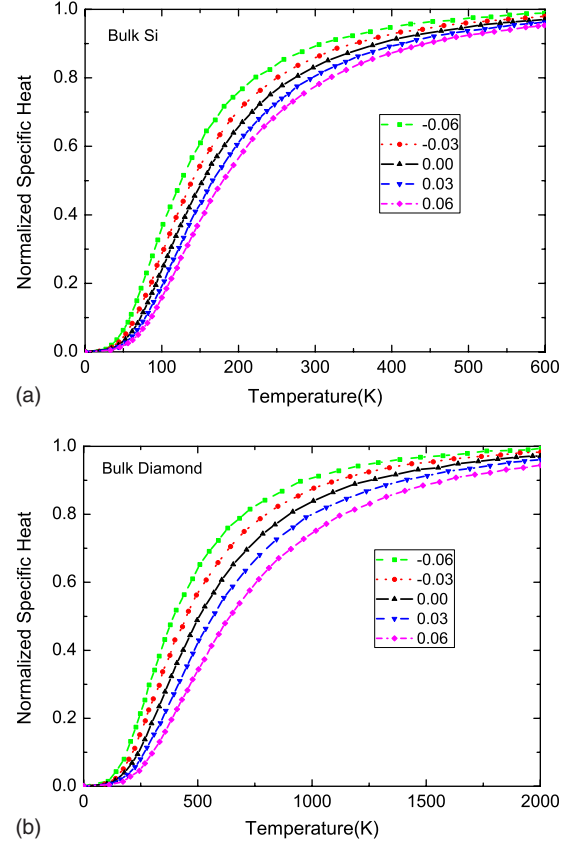
bulk and nanoforms using the method developed in previous section. Under periodic boundary conditions, strain is applied simply by changing the lattice constant according to the zero-strain value determined in Sec. II A. For bulk materials, same strains are applied uniaxially in the three directions. For thin film, strains are applied in the thin-film plane (*Y* and *Z* directions) and for nanowires the strain is applied in the axial *Z* direction. During the simulation, the simulation-domain size is changed according to the strain along the direction where strain is applied and in other directions the system is relaxed with free boundary condition. With this method, the strain/stress field inside the simulated materials is very complicated. To make the discussion simple, we used the applied strain when presenting the results in this work.

Since the structures are expected to deform under large strain, the volume is determined from the structures via the coordinates output. For nanowires, the cross-sectional area is determined from the final structure and volume is taken as the product of the length and the cross-sectional area. For thin films, the volume is taken as the product of average film thickness and the area. For nanowires and thin films, a finite atom thickness (1/4 of one unit-cell size) at the boundary is accounted when calculating the volume. This is consistent with the calculation of the simulation-domain volume when periodic boundary condition is applied. For both carbon
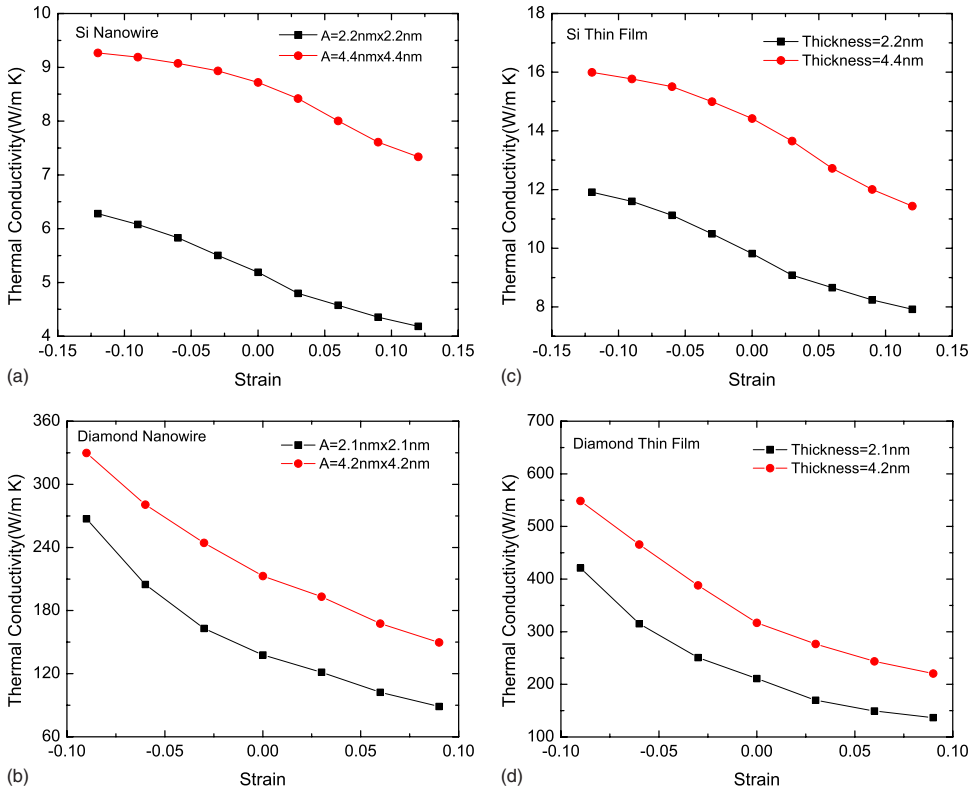
FIG. 8. (Color online) Strain effects on the thermal conductivity of: (a) silicon nanowires, (b) diamond nanowires, (c) silicon thin films, and (d) diamond thin films.

nanotubes and graphene sheets, the volume is taken as the product of the surface area and a thickness of 3.4 Å which is usually used as the equilibrium distance between two graphene layers. Thermal conductivity is calculated in the direction where strain is applied and results are shown in the following sections.

A. Bulk silicon and diamond

We first studied the strain effects on thermal conductivity of bulk silicon and diamond. Same strain is applied uniaxially in three directions with periodic boundary conditions. The results are shown in Fig. 5 for the thermal conductivity as a function of the applied strain, where the nondimensional strain is defined as the change in the length per unit of the original length at the directions where the stress is applied. For both bulk silicon and carbon (diamond), thermal conductivity decreases continuously from compressive strain to tensile strain. This trend agrees well with the simulation results on bulk argon which used Lennard-Jones potential from Ref. 34–36. From the kinetic theory, thermal conductivity can be expressed as $k=\frac{1}{3}\Sigma_{k,p}C_{k,p}v_{k,p}\lambda_{k,p}$, where C is the specific heat, v is average phonon group velocity, and λ is phonon mean-free path of each phonon mode (subscript k, p). We investigated the change in specific heat and group velocity by calculating the dispersion curve of these two materials under different strains, as shown in Fig. 6. Under compressive strains, phonon-dispersion curves shift upward which results in a larger phonon group velocity of the acoustic phonons ($v_g = \partial\omega/\partial k$). Such a shift of the phonon-dispersion curve will result in both the increase in the specific heat of each modes and the total specific heat as shown in Fig. 7.

Under tensile strain, the trend goes to the opposite direction and both phonon group velocity and specific heat decrease. These two effects will result in a decreasing thermal conductivity from compressive strain to tensile one. From the figure, it also shows that strain affects more on the longitude-acoustic phonon than transverse-acoustic phonons.

We note that the maximum strain which the materials can stand before cracking from MD simulation is much larger than the real material. This is because: (1) the empirical potential (Tersoff potential) is derived by fitting the physical properties at zero pressure and the applicability to extremely high-pressure simulation is limited; (2) the structures studied here are perfect crystals and the lattice spacing only changes proportionally to the applied strain, which means an initial crack point is hard to form for crack propagation.

B. Nanowires and thin films

Figure 8 shows the calculated thermal conductivity of Si and diamond nanowires and thin films under different applied strains. Similar trends as that of bulk materials are observed on the change in thermal conductivity when the applied strain changes. The reason is that the phonon-dispersion curve shift in Fig. 6 is mainly due to the material stiffness change under strain. For nanowires under strain, similar stiffness change and the phonon-dispersion curve shift trends could be obtained comparing with the bulk material. We also note that we used small number of unit cells for the simulation due to the high computational cost of Tersoff potential in MD simulation. The decision of using small number of unit cells is based on the converging results of spectral method as discussed in Figs. 2 and 3.
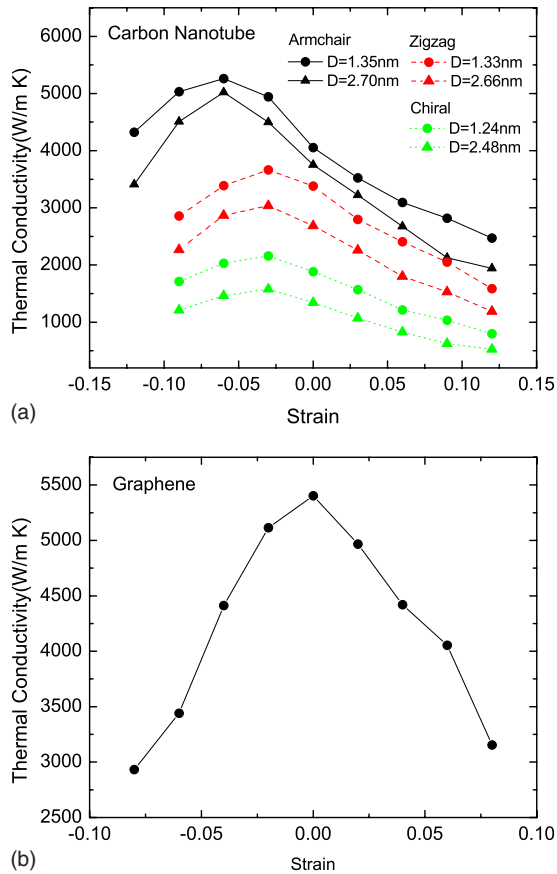
FIG. 9. (Color online) Thermal conductivity of: (a) SWCNTs and (b) single-layer graphene, as a function of applied strain. Two diameters are studied for armchair, zigzag, and chiral-type SWCNTs: ~1.3 nm and ~2.6 nm.

FIG. 10. (Color online) (a) Structures of (10, 10) armchair SWCNT (diameter=1.35 nm) and (b) single graphene sheet under strain.

C. Carbon nanotubes and single-layer graphene

Figure 9 shows the strain effects on thermal conductivity of SWCNTs and single-layer graphene. Three different types of SWCNT with similar diameter are studied: armchair, zigzag, and chiral SWCNTs, among which the armchair SWCNT has the highest thermal conductivity and the chiral SWCNT has the lowest thermal conductivity. We observed the thermal conductivity of SWCNT and graphene decreases under certain compressive strain, as shown in Fig. 8, which is significantly different from silicon and carbon nanowires, and thin films that are discussed above and the previous NEMD simulation for carbon nanotubes under compressive and tensile pressure.[37] The peak thermal conductivity occurs at −0.06 for armchair SWCNT, −0.03 for zigzag and chiral SWCNT. Interestingly the highest thermal conductivity of graphene is obtained when it is subject to no applied strain.

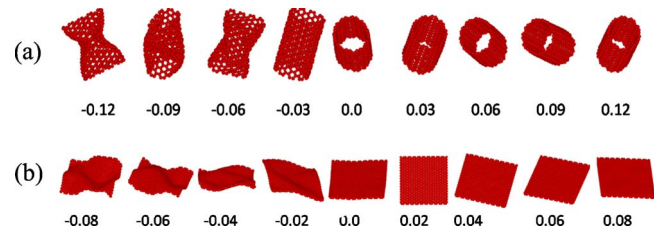To explain the existence of the peak thermal conductivity, we plot in Fig. 10 the deformation of the SWCNT and single graphene sheet. It clearly shows that the SWCNT and single graphene sheet buckle when the applied strain is compressive. The buckling is due to the hollow structure of SWCNTs and the single atomic layer nature of the graphene sheet. When SWCNT and single graphene sheet buckles under compressive strain, more irregular surfaces are created and phonons can be scattered significantly more often. Therefore, we would expect a reduction in thermal conductivity of SWCNTs and single graphene sheet when they buckle under applied compressive strain. However, we could expect a trend occurring in SWCNT and graphene similar to that of the nanowires and thin film when they are under tensile stress due to the phonon-dispersion curve shift.

IV. CONCLUSIONS

In this paper, strain effects on the lattice thermal conductivity have been studied systematically for bulk and low-dimensional silicon and carbon nanostructures (silicon and diamond nanowire, silicon and diamond thin films, SWCNT and single graphene sheet). The thermal conductivity of the silicon and diamond nanowires and thin films decreases continuously when the applied strain is changed from compressive to tensile, due to the shift of phonon-dispersion curves under strains. However, due to the single-layer nature of SWCNT and single-layer graphene sheet, buckling occurs when large compressive strain is applied. The bucking results in an increasing phonon scattering rate and thus a reduced thermal conductivity under compressive strains. Overall, the thermal conductivity of nanostructures can be greatly tuned by applying strain/stress. For example, the thermal conductivity of (10, 10) SWCNT varies from 60% to 130% under strain comparing to the value of a free-standing one. Strain/stress tuning of the thermal conductivity of nanostructures can have lots of applications and implications on thermal management and energy conversion.

ACKNOWLEDGMENTS

*Corresponding author; ronggui.yang@colorado.edu

[1] J. Hone, M. Whitney, C. Piskoti, and A. Zettl, Phys. Rev. B **59**, R2514 (1999).

[2] D. G. Cahill, W. K. Ford, K. E. Goodson, G. D. Mahan, A. Majumdar, H. J. Maris, R. Merlin, and S. R. Phillpot, J. Appl. Phys. **93**, 793 (2003).

[3] R. G. Yang and G. Chen, Phys. Rev. B **69**, 195316 (2004); R. G. Yang, G. Chen, and M. S. Dresselhaus, *ibid.* **72**, 125418 (2005); Nano Lett. **5**, 1111 (2005); W. X. Tian and R. G. Yang, J. Appl. Phys. **101**, 054320 (2007); M. S. Jeng, R. G. Yang, D. W. Song, and G. Chen, J. Heat Transfer **130**, 042410 (2008); M. E. Siemens, Q. Li, R. Yang, K. A. Nelson, E. H. Anderson, M. M. Murnane, and H. C. Kapteyn, Nature Mater. **9**, 26 (2010); A. Evgrafov, K. Maute, R. G. Yang, and M. L. Dunn, Int. J. Numer. Methods Eng. **77**, 285 (2009).

[4] T. Yao, Appl. Phys. Lett. **51**, 1798 (1987).

[5] G. Chen, C. L. Tien, X. Wu, and J. S. Smith, J. Heat Transfer **116**, 325 (1994).

[6] S. M. Lee, D. G. Cahill, and R. Venkatasubramanian, Appl. Phys. Lett. **70**, 2957 (1997).

[7] A. Vassighi and M. Sachdev, *Thermal and Power Management of Integrated Circuits* (Springer, New York, 2006).

[8] R. S. Prasher, J. Y. Chang, I. Sauciuc, S. Narasimhan, D. Chau, G. Chrysler, A. Myers, S. Prstic, and C. Hu, Intel Technol. J. **9**, 285 (2005); R. S. Prasher, Proc. IEEE **94**, 1571 (2006).

[9] M. S. Dresselhaus, G. Chen, M. Y. Tang, R. G. Yang, H. Lee, D. Z. Wang, Z. F. Ren, J.-P. Fleurial, and P. Gogna, Adv. Mater. **19**, 1043 (2007); B. Poudel, Q. Hao, Y. Ma, Y. C. Lan, A. Minnich, B. Yu, X. Yan, D. Z. Wang, A. Muto, D. Vashaee, X. Y. Chen,
J. M. Liu, M. S. Dresselhaus, G. Chen, and Z. F. Ren, Science **320**, 634 (2008); S. J. Thiagarajan, W. Wang, and R. G. Yang, Annu. Rev. Nano Res. **3**, 447 (2009).

[10] T. C. Harman, P. J. Taylor, M. P. Walsh, and B. E. LaForge, Science **297**, 2229 (2002).

[11] P. Poizot, S. Laruelle, S. Grugeon, L. Dupont, and J.-M. Tarascon, Nature (London) **407**, 496 (2000).

[12] P. Peumans, S. Uchida, and S. R. Forrest, Nature (London) **425**, 158 (2003).

[13] W. Chang, D. Okawa, A. Majumdar, and A. Zettl, Science **314**, 1121 (2006).

[14] N. Yang, G. Zhang, and B. Li, Appl. Phys. Lett. **93**, 243111 (2008).

[15] T. Ruokola, T. Ojanen, and A. P. Jauho, Phys. Rev. B **79**, 144306 (2009).

[16] B. Li, L. Wang, and G. Casati, Phys. Rev. Lett. **93**, 184301 (2004).

[17] C. Dames, J. Heat Transfer **131**, 061301 (2009).

[18] K. Ismail, S. F. Nelson, J. O. Chu, and B. S. Meyerson, Appl. Phys. Lett. **63**, 660 (1993).

[19] Y. J. Mii, Y. H. Xie, E. A. Fitzgerald, D. Monroe, F. A. Thiel, and E. B. Weir, Appl. Phys. Lett. **59**, 1611 (1991); M. Chu, Y. Sun, U. Aghoram, and S. E. Thompson, Annu. Rev. Mater. Res. **39**, 203 (2009).

[20] T. Vogelsang and K. R. Hofmann, Appl. Phys. Lett. **63**, 186 (1993).

[21] O. Stier, M. Grundmann, and D. Bimberg, Phys. Rev. B **59**, 5688 (1999).

[22] R. Ghosh, D. Basak, and S. Fujihara, J. Appl. Phys. **96**, 2689 (2004).

[23] M. Suzuki and T. Uenoyama, J. Appl. Phys. **80**, 6868 (1996).

[24] S. Y. Kim and H. S. Park, Phys. Rev. Lett. **101**, 215502 (2008).

[25] J. F. Meng, N. V. Chandra Shekar, and J. V. Badding, J. Appl. Phys. **90**, 2836 (2001).

[26] D. A. Polvani, J. F. Meng, N. V. Chandra Shekar, J. Sharp, and J. V. Badding, Chem. Mater. **13**, 2068 (2001).

[27] R. G. Ross, P. Andersson, B. Sundquist, and G. Bäckström, Rep. Prog. Phys. **47**, 1347 (1984).

[28] P. I. Baranskii, P. P. Kogutyuk, and V. V. Sabyak, Sov. Phys. Semicond. **15**, 1061 (1981).

[29] P. W. Bridgman, Am. J. Sci. **7**, 81 (1924).

[30] A. A. Averkin, Z. Z. Zhaparov, and L. S. Stil'bans, Sov. Phys. Semicond. **5**, 1954 (1972).

[31] Kh. I. Amirkhanov, Ya. B. Magomedov, and S. N. Emirov, Sov. Phys. Solid State **15**, 1015 (1973).

[32] R. G. Ross and O. Sandberg, J. Phys. C **11**, 667 (1978).

[33] P. Andersson, R. G. Ross, and G. Backstrom, J. Phys. C **13**, L73 (1980).

[34] H. Kaburaki, J. Li, and S. Yip, *Multiscale Modeling of Material*, MRS Symposia Proceedings (Materials Research Society, Pittsburgh, 1999).

[35] R. C. Picu, T. Borca-Tasciuc, and M. C. Pavel, J. Appl. Phys. **93**, 3535 (2003).

[36] S. Bhowmick and V. B. Shenoy, J. Chem. Phys. **125**, 164513 (2006).

[37] H. Fan, K. Zhang, and M. M. F. Yuen, in Proceedings of the International Conference on Thermal, Mechanical and Multi-Physics Simulation Experiments in Micro-Electronics and Micro-Systems, 2007, London (IEEE, 2007).

[38] A. R. Abramson, C. L. Tien, and A. Majumdar, J. Heat Transfer **124**, 963 (2002).

[39] I. Rosenblum, J. Adler, S. Brandon, and A. Hoffman, Phys. Rev. B **62**, 2920 (2000).

[40] S. G. Volz and G. Chen, Phys. Rev. B **61**, 2651 (2000).

[41] N. Mingo and L. Yang, Phys. Rev. B **68**, 245406 (2003).

[42] D. C. Rapaport, *The Art of Molecular Dynamics Simulation* (Cambridge University Press, Cambridge, England, 1998).

[43] G. Box and M. Muller, Ann. Math. Stat. **29**, 610 (1958).

[44] W. C. Swope, H. C. Anderson, P. H. Berens, and K. R. Wilson, J. Chem. Phys. **76**, 637 (1982).

[45] R. Kubo, M. Toda, and N. Hashitsume, *Statistical Physics* (Springer, Berlin, 1985), Vol. II.

[46] G. D. Mahan, *Many-Particle Physics* (Plenum, New York, 1993).

[47] F. H. Stillinger and T. A. Weber, Phys. Rev. B **31**, 5262 (1985).

[48] J. Tersoff, Phys. Rev. B **39**, 5566 (1989).

[49] J. Q. Broughton and X. P. Li, Phys. Rev. B **35**, 9120 (1987).

[50] S. J. Cook and P. Clancy, Phys. Rev. B **47**, 7686 (1993).

[51] J. Fabian and P. B. Allen, Phys. Rev. Lett. **79**, 1885 (1997).

[52] L. J. Porter, S. Yip, M. Yamaguchi, H. Kaburaki, and M. Tang, J. Appl. Phys. **81**, 96 (1997).

[53] J. D. Schall, P. T. Mikulski, G. M. Chateauneuf, G. Gao, and J. A. Harrison, in *Superlubricity*, edited by A. Erdemir and J.-M. Martin (Elsevier, Amsterdam, The Netherlands, 2007), pp. 85–86.

[54] B. W. Dodson, Phys. Rev. B **33**, 7361 (1986).

[55] *Physics of Group IV Elements and III-V Compounds*, Landolt-Börnstein, New Series, Group III, edited by O. Madelung, M. Schulz, and H. Weiss (Springer-Verlag, Berlin, 1995), p. 21.

[56] A. J. H. McGaughey and M. Kaviany, Int. J. Heat Mass Transfer **47**, 1783 (2004).

[57] A. J. H. McGaughey and M. Kaviany, Int. J. Heat Mass Transfer **47**, 1799 (2004).

[58] P. K. Schelling, S. R. Phillpot, and P. Keblinski, Phys. Rev. B **65**, 144306 (2002).

[59] J. Che, T. Cagin, W. Deng, and W. A. Goddard III, J. Chem. Phys. **113**, 6888 (2000).

[60] J. Li, L. J. Porter, and S. Yip, J. Nucl. Mater. **255**, 139 (1998).

[61] T. Kawamura, D. Hori, Y. Kangawa, K. Kakimoto, M. Yoshimura, and Y. Mori, Jpn. J. Appl. Phys. **47**, 8898 (2008).

[62] M. Grujicic, G. Cao, and B. Gersten, Mater. Sci. Eng., B **107**, 204 (2004).

[63] Y. H. Lee, R. Biswas, C. M. Soukoulis, C. Z. Wang, C. T. Chan, and K. M. Ho, Phys. Rev. B **43**, 6573 (1991).

[64] S. G. Volz, Phys. Rev. Lett. **87**, 074301 (2001).

[65] Y. K. Koh and D. G. Cahill, Phys. Rev. B **76**, 075207 (2007).

[66] T. Ruf, R. W. Henn, M. Asen-Palmer, E. Gmelin, M. Cardona, H.-J. Pohl, G. G. Devyatych, and P. G. Sennikov, Solid State Commun. **115**, 243 (2000).

[67] L. Wei, P. K. Kuo, and R. L. Thomas, Phys. Rev. Lett. **70**, 3764 (1993).

[68] S. Lepri, R. Livi, and A. Politi, Europhys. Lett. **43**, 271 (1998).

[69] S. Wang, X. Liang, X. Xu, and T. Oh ara, J. Appl. Phys. **105**, 014316 (2009).

[70] S. Lepri, R. Livi, and A. Politi, Phys. Rep. **377**, 1 (2003).